
TASAC: Temporally Abstract Soft Actor-Critic for Continuous Control

Haonan Yu¹ Wei Xu¹ Haichao Zhang¹

Abstract

We propose temporally abstract soft actor-critic (TASAC), an off-policy RL algorithm that incorporates closed-loop temporal abstraction into the soft actor-critic (SAC) framework in a simple manner. TASAC adds a second-stage binary policy to choose between the previous action and the action output by an SAC actor. It has two benefits compared to traditional off-policy RL algorithms: persistent exploration and an unbiased multi-step Q operator for TD learning. We demonstrate its advantages over several strong baselines across 5 different categories of 14 continuous control tasks, in terms of both sample efficiency and final performance. Because of its simplicity and generality, TASAC can serve as a drop-in replacement for SAC when temporal abstraction is needed. Code is available at <https://github.com/hnyu/tasac>.

1. Introduction

Deep reinforcement learning (RL) has achieved great success in various continuous action domains such as locomotion and manipulation (Schulman et al., 2015; Lillicrap et al., 2016; Duan et al., 2016; Schulman et al., 2017; Fujimoto et al., 2018; Haarnoja et al., 2018). Despite promising empirical results, these widely applicable continuous RL algorithms execute a newly computed action at every step of the finest time scale of a problem. With no decision making at higher levels, they attempt to solve the challenging credit assignment problem over a long horizon. As a result, considerable sample efficiency improvements have yet to be made by them in complex task structures (Riedmiller et al., 2018; Li et al., 2020; Lee et al., 2020b) and extremely sparse reward settings (Andrychowicz et al., 2017; Plappert et al., 2018; Zhang et al., 2021).

On the other hand, it is argued that temporal abstraction (Parr & Russell, 1998; Dietterich, 1998; Sutton et al., 1999; Precup, 2000) is one of the crucial keys to solving control

problems with complex structures. The action hierarchy formed by temporal abstraction could serve as a useful prior aligned with the complex task structure, or encourage exploration for discovering sparse rewards, as larger steps are taken at higher levels of abstraction while lower-level actions only need to focus on solving isolated subtasks (Dayan & Hinton, 1993; Vezhnevets et al., 2017; Bacon et al., 2017). However, most hierarchical RL methods are task specific or nontrivial to adapt. For example, the options framework (Sutton et al., 1999; Precup, 2000; Bacon et al., 2017) requires pre-defining an option space, while the feudal RL framework (Vezhnevets et al., 2017; Nachum et al., 2018; Zhang et al., 2021) requires tuning the hyperparameters of dimensionality and domain range of the goal space for every different task. In practice, their final performance usually hinges on these choices. Moreover, learning sub-policies and their termination conditions from scratch could be expensive in terms of data and computation. As a result, some hierarchical methods (Riedmiller et al., 2018; Lee et al., 2020b) use pre-trained skills or sub-policies to facilitate training, assuming a known task structure. This somewhat limits their generalization to new scenarios.

Perhaps the simplest form of an option or sub-policy would be just repeating an action for a certain number of steps, a straightforward idea that has been explored before (Lakshminarayanan et al., 2017; Sharma et al., 2017; Dabney et al., 2021; Metelli et al., 2020; Lee et al., 2020a). This line of works can be regarded as a middle ground between “flat” and hierarchical RL. Nevertheless, they all assume a fixed candidate set of action durations, and repeat actions in an *open-loop* manner. Open-loop control forces an agent to commit to the same action over a pre-determined duration with no early termination. It weakens the agent’s ability of handling emergency situations and correcting wrong durations predicted earlier. Given a new task, it is nontrivial to define the duration candidate set while balancing the trade-off between temporal abstraction and optimal control.

In this paper, our goal is to keep the simplicity of “flat” RL while modeling lightweight temporal abstraction. Simplicity promotes a wide range of applications of a method due to few assumptions or moving parts. Meanwhile, a lightweight instantiation of temporal abstraction could suffice to boost the performance of traditional “flat” RL methods. We propose temporally abstract soft actor-critic

¹Horizon Robotics, California, USA. Correspondence to: Haonan Yu <haonan.yu@horizon.ai>.

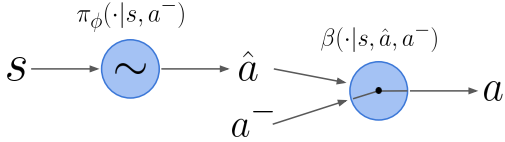


Figure 1. An illustration of TASAC’s two-stage policy during inference. In the first stage, an action policy π_ϕ (SAC actor) samples a candidate action \hat{a} . In the second stage, a binary switching policy β chooses between this candidate and the previous action a^- .

(TASAC), an off-policy RL algorithm that incorporates *closed-loop* action repetition into a soft actor-critic (SAC) framework (Haarnoja et al., 2018). TASAC is conceptually simple and only requires a slight modification to SAC. Generally, for inference we add a second stage that chooses between a candidate action output by an SAC actor and the action from the previous step (Figure 1). For policy evaluation, we propose a new *unbiased* multi-step Q operator for TD backup by re-using trajectories that have shared repeated actions between rollout and training. For policy improvement, we show that the new actor gradient can be approximated by multiplying a scaling factor to the $\frac{\partial Q}{\partial a}$ term in the original SAC’s actor gradient, where the scaling factor is the optimal probability of choosing the candidate action in the second stage (Eq. 8).

TASAC is much easier to train compared to sophisticated hierarchical methods. At the same time, it has two benefits compared to “flat” off-policy RL algorithms. First, TASAC encourages *persistent exploration* because the second stage is able to repeat the same continuous action persistently with a non-zero probability. Second, TASAC bootstraps Q values across multiple steps to speed up policy evaluation.

One recent work closest to TASAC is PIC (Chen et al., 2021) which also learns to repeat the last action to address the action oscillation issue within consecutive steps during online execution. There are at least three major differences between TASAC and PIC. First, PIC was proposed for discrete control and its extension to continuous control is unclear yet. Second, PIC predicts whether to repeat the last action *before* a new candidate action is sampled. This requires its switching policy to make a decision regardless of their core policy’s output. Lastly, PIC employs a nested SAC training procedure which is far more complex than TASAC’s.

We evaluate TASAC on 5 different categories of 14 continuous control tasks, covering simple control, locomotion, terrain walking, manipulation, and self-driving (Brockman et al., 2016; Plappert et al., 2018; Dosovitskiy et al., 2017). Averaged over these tasks, TASAC outperforms 5 strong baselines by large margins of normalized score, in terms of both sample efficiency and final performance. Because of its simplicity, TASAC could serve as a drop-in replacement for SAC in continuous control for temporal abstraction.

2. Preliminaries

We consider the RL problem as policy search in a Markov Decision Process (MDP). Let $s \in \mathbb{R}^M$ denote a state, where a continuous action $a \in \mathbb{R}^A$ is taken. Let $\pi(a|s)$ be the action policy, and $\mathcal{P}(s_{t+1}|s_t, a_t)$ the probability of the environment transitioning to s_{t+1} after an action a_t is taken at s_t . Upon reaching s_{t+1} , the agent receives a scalar reward $r(s_t, a_t, s_{t+1})$. Assuming an initial state $s_0 \sim \mathcal{P}(s_0)$, the RL objective is to find a policy π^* that maximizes the expected discounted return: $\mathbb{E}_{\pi, \mathcal{P}} [\sum_{t=0}^{\infty} \gamma^t r(s_t, a_t, s_{t+1})]$, where $\gamma \in (0, 1)$ is a discount factor. We further define $Q^\pi(s_t, a_t) = \mathbb{E}_\pi [\sum_{t'=t}^{\infty} \gamma^{t'-t} r(s_{t'}, a_{t'}, s_{t'+1})]$ as the discounted return starting from s_t given that a_t is taken, and $V^\pi(s_t) = \mathbb{E}_{a_t \sim \pi} Q^\pi(s_t, a_t)$ as the state value of s_t . We denote the marginal state visitation distribution by $\rho^\pi(s)$, then the RL objective can also be written as $\mathbb{E}_{s \sim \rho^\pi, a \sim \pi} Q^\pi(s, a)$.

However, computing $\rho^\pi(s)$ is usually intractable. As a result, in an off-policy actor-critic setting with π and Q parameterized by ϕ and θ , the objective is sometimes modified (Lillicrap et al., 2016; Haarnoja et al., 2018) as

$$\max_{\phi} \mathbb{E}_{s \sim \mathcal{D}} V_{\theta}^{\pi_\phi}(s) = \max_{\phi} \mathbb{E}_{s \sim \mathcal{D}, a \sim \pi_\phi} Q_{\theta}(s, a). \quad (1)$$

This assumes that 1) s is sampled from a replay buffer instead of the current policy, and 2) the dependency of the critic Q on the policy π_ϕ is dropped when computing the gradient of ϕ . Meanwhile, θ is learned separately via policy evaluation with typical temporal-difference (TD) backups.

If π_ϕ is stochastic, a re-parameterization trick $a = f_\phi(s, \epsilon)$ (ϵ is a noise vector e.g., $\mathcal{N}(0, 1)$) can be applied to Eq. 1:

$$\max_{\phi} \mathbb{E}_{s \sim \mathcal{D}, \epsilon} Q_{\theta}(s, f_{\phi}(s, \epsilon)).$$

Based on this, SAC (Haarnoja et al., 2018) adopts the maximum entropy (MaxEnt) framework (Ziebart, 2010) that augments the V value function with action entropy:

$$V_{\theta}^{\pi_\phi}(s) = \mathbb{E}_{a \sim \pi_\phi} [Q_{\theta}(s, a) - \alpha \log \pi_{\phi}(a|s)],$$

where the entropy term encourages exploration and prevents premature convergence. This formulation essentially adds entropy as a bonus reward to the environment reward.

3. Temporally abstract soft actor-critic

To enable temporal abstraction, we motivate a decomposition of the agent’s action decision into two stages: 1) sampling a new candidate action $\hat{a} \sim \pi_\phi(\cdot|s, a^-)$ conditioned on the action a^- at the previous time step, and 2) choosing between a^- and \hat{a} for the actual output at the current step.

3.1. Two-stage policy

Formally, let $\beta(b|s, \hat{a}, a^-)$ be the binary switching policy, where $b = 0$ means choosing a^- and $b = 1$ oth-

Algorithm 1: Temporally abstract soft actor-critic

Input: θ, ϕ, λ (learning rate), and τ (moving average rate)
Initialize: Randomize θ and ϕ , $\bar{\theta} \leftarrow \theta$, $\mathcal{D} \leftarrow \emptyset$
for each training iteration do
 for each rollout step do
 $\hat{a} \sim \pi_\phi(\hat{a}|s, a^-)$ \triangleright first-stage policy
 $b \sim \beta_b^*$ (Eq. 6) \triangleright second-stage policy
 $a \leftarrow a^-$ if $b = 0$ else $a \leftarrow \hat{a}$
 $s' \sim \mathcal{P}(s'|s, a)$
 $\mathcal{D} \leftarrow \mathcal{D} \cup \{(a^-, s, a, s', r(s, a, s'))\}$
 $(s, a^-) \leftarrow (s', a)$
 end
 for each gradient step do
 $\theta \leftarrow \theta - \lambda \Delta \theta$ (grad of Eq. 4 with $\mathcal{T}^{\pi^{\text{ta}}}$) \triangleright
 policy evaluation
 $\phi \leftarrow \phi + \lambda \Delta \phi$ (Eq. 8) \triangleright policy
 improvement
 $\alpha \leftarrow \alpha - \lambda \Delta \alpha$ (grad of Eq. 9) $\triangleright \alpha$
 adjustment
 $\bar{\theta} \leftarrow \bar{\theta} + \tau(\theta - \bar{\theta})$ \triangleright target network update
 end
end
Output: θ and ϕ

erwise. For simplicity, in the following we will denote $\beta_b = \beta(b|s, \hat{a}, a^-)$ (always assuming its dependency on s , \hat{a} , and a^-). Then our two-stage policy π^{ta} is defined as

$$\begin{aligned} \pi^{\text{ta}}(a|s, a^-) &\triangleq \int_{\hat{a}} \pi_\phi(\hat{a}|s, a^-) P(a|s, \hat{a}, a^-) d\hat{a} \quad (\text{marginal over } \hat{a}) \\ &\triangleq \int_{\hat{a}} \pi_\phi(\hat{a}|s, a^-) [\beta_0 \delta(a - a^-) + \beta_1 \delta(a - \hat{a})] d\hat{a}, \end{aligned} \quad (2)$$

which can be shown to be a proper probability distribution of a . This two-stage policy repeats previous actions through a binary policy β , a decision maker that compares a^- and \hat{a} side by side given the current state s . Repeatedly favoring $b = 0$ results in temporal abstraction of executing the same action for multiple steps. Moreover, this control is closed-loop, as it does not commit to a pre-determined time window; instead it can stop repetition whenever necessary. As a special case, when $\beta_1 = 1$, π^{ta} reduces to π_ϕ ; when $\beta_0 = 1$, $\pi^{\text{ta}}(a|s, a^-) = \delta(a - a^-)$.

It can be shown (Appendix A) that the parameterized state value function of π^{ta} is

$$\begin{aligned} V_\theta^{\pi^{\text{ta}}}(s|a^-) &= \mathbb{E}_{\hat{a} \sim \pi_\phi, b \sim \beta} Q_\theta(s, a^-, \hat{a}, b), \\ \text{with } Q_\theta(s, a^-, \hat{a}, b) &\triangleq (1 - b)Q_\theta(s, a^-) + bQ_\theta(s, \hat{a}). \end{aligned} \quad (3)$$

Intuitively, the actual Q value of each $a \sim \pi^{\text{ta}}$ is an interpolation by β between the Q values of a^- and \hat{a} . This

is consistent with our motivation: if a^- is taken, by the Q definition the future discounted return is just $Q(s, a^-)$, otherwise $Q(s, \hat{a})$. Note that unlike SAC (Haarnoja et al., 2018) here we choose not to add entropy as a bonus reward in $V_\theta^{\pi^{\text{ta}}}$. Instead, entropy will be used merely as a regularization term for policy improvement (Section 3.3)¹. This choice can be justified by a recent work (Wang et al., 2020) which shows that the major contribution of the entropy term in SAC is to resolve the action squashing problem during actor optimization. With our two-stage policy defined, next we describe how to perform policy evaluation for learning Q_θ (Section 3.2) and policy improvement for learning π^{ta} (Section 3.3). The overall TASAC algorithm is summarized in Algorithm 1.

3.2. Policy evaluation

The typical TD learning objective for a policy π is

$$\begin{aligned} \min_{\theta} \mathbb{E}_{(s, a, s') \sim \mathcal{D}} [Q_\theta(s, a) - \mathcal{B}^\pi Q_\theta(s, a)]^2, \\ \text{with } \mathcal{B}^\pi Q_\theta(s, a) = r(s, a, s') + \gamma V_\theta^\pi(s'), \end{aligned} \quad (4)$$

where the Bellman operator \mathcal{B}^π allows one-step bootstrapping, and $\bar{\theta}$ slowly tracks θ to stabilize the learning (Mnih et al., 2015). Below we first propose a new multi-step Q operator that allows more efficient policy evaluation for any *action-reproducible* policy. In an off-policy training setting, we define a policy to be action-reproducible if at each rollout state with a non-zero probability it generates an action that is *identical* to the rollout action. Then we explain how our two-stage policy, as a continuous policy, is action-reproducible and qualified for this new operator.

Given any trajectory $(s_0, a_0, s_1, a_1, \dots, s_N)$ of $N + 1$ steps sampled from a replay buffer, typically we cannot directly use s_n ($n \geq 2$) as the target state in TD backup because it is sampled from a different behavior policy. Our proposed multi-step Q operator \mathcal{T}^π proceeds as follows. Let $(\tilde{a}_1, \tilde{a}_2, \dots, \tilde{a}_N)$ denote the actions sampled from π at states (s_1, s_2, \dots, s_N) . Starting from $n = 1$, we compare \tilde{a}_n with a_n one by one. If $\tilde{a}_n = a_n$, then we set $n \leftarrow n + 1$. We keep comparing until $\tilde{a}_n \neq a_n$ or $n = N$. Finally, our multi-step operator is defined as

$$\mathcal{T}^\pi Q_\theta(s_0, a_0) = \sum_{t=0}^{n-1} \gamma^t r(s_t, a_t, s_{t+1}) + \gamma^n Q_\theta(s_n, \tilde{a}_n).$$

In Appendix H we give a formal definition of \mathcal{T}^π and prove that Q^π is its unique fixed point. This suggests that when applying \mathcal{T}^π to Eq. 4, Q_θ will be driven to fit Q^π .

¹Strictly speaking, our two-stage policy π^{ta} is no longer ‘‘soft’’ as its value does not include the entropy reward. But we still call the proposed algorithm ‘‘TASAC’’ to remind that its overall training framework is very analogous to SAC’s.

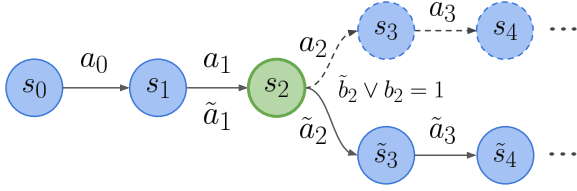


Figure 2. An illustration of multi-step TD learning by exploiting action repetition of π^{ta} . The upper branch is the trajectory sampled by a rollout policy; the lower one is sampled by the current policy during training. We have $\tilde{a}_1 = a_1 = a_0$ due to $b_1 = \tilde{b}_1 = 0$. The two trajectories diverge at s_2 because either $b_2 = 1$ or $\tilde{b}_2 = 1$. For bootstrapping, we use s_2 as the target state in this example.

A typical continuous policy such as used by DDPG (Lillicrap et al., 2016) or SAC (Haarnoja et al., 2018) is not action-producible ($\tilde{a}_n \neq a_n$ with a probability of 1). Thus n always stops at 1 and \mathcal{T}^π seems no more than just a Bellman operator \mathcal{B}^π . However, if a continuous policy is specially structured to be action-reproducible, it will enjoy the privilege of using s_n ($n > 1$) as the target state. Our two-stage π^{ta} is such an example. In our case, each action a_n (\tilde{a}_n) is accompanied by a repeating choice output b_n (\tilde{b}_n). Starting from $n = 1$, if $\tilde{b}_n = b_n = 0$ (both repeated), then we know that $\tilde{a}_n = a_n = a_0$. See Figure 2 for an illustration. Thus for more efficient policy evaluation we use $\mathcal{T}^{\pi^{\text{ta}}}$ as our multi-step Q operator to replace \mathcal{B}^π in Eq. 4.

Remark on the new multi-step operator The proposed operator \mathcal{T}^π is certainly not meant to replace multi-step TD learning with importance correction (Munos et al., 2016) in a general scenario, as it is only valid for action-reproducible policies. Also its actual effective bootstrapping step is usually limited by checking $\tilde{a}_n \neq a_n$ to be smaller than the maximal bootstrapping step N .

3.3. Policy improvement

With π^{ta} possibly repeating previous actions a^- , our policy improvement objective adapted from Eq. 1 becomes

$$\max_{\phi, \beta} \mathbb{E}_{(s, a^-) \sim \mathcal{D}} V_{\theta}^{\pi^{\text{ta}}}(s|a^-).$$

Notice that each time we also sample the previous action a^- along with a state s from the replay buffer. To encourage exploration and prevent premature policy convergence, we augment this objective with the joint entropy \mathcal{H}_{s, a^-} for regularization. The joint entropy is computed as

$$\begin{aligned} \mathcal{H}_{s, a^-} &= - \mathbb{E}_{P(\hat{a}, b|s, a^-)} \log P(\hat{a}, b|s, a^-) \\ &= - \mathbb{E}_{\pi_{\phi}(\hat{a}|s, a^-) \beta_b} [\log \pi_{\phi}(\hat{a}|s, a^-) + \log \beta_b] \end{aligned}$$

Thus the final policy improvement object is

$$\begin{aligned} &\max_{\phi, \beta} \mathbb{E}_{(s, a^-) \sim \mathcal{D}} [V_{\theta}^{\pi^{\text{ta}}}(s|a^-) + \alpha \mathcal{H}_{s, a^-}] \\ &= \max_{\phi, \beta} \mathbb{E}_{(s, a^-) \sim \mathcal{D}, \hat{a} \sim \pi_{\phi}, b \sim \beta} \begin{bmatrix} Q_{\theta}(s, a^-, \hat{a}, b) \\ -\alpha \log \beta_b \\ -\alpha \log \pi_{\phi}(\hat{a}|s, a^-) \end{bmatrix}, \end{aligned} \quad (5)$$

where α is a temperature. To maximize this objective with respect to β , one can parameterize β and use stochastic gradient ascent. However, for every sampled (s, a^-, \hat{a}) , there is in fact a closed-form solution (see Appendix B for derivation details) for the innermost expectation over $b \sim \beta$:

$$\beta_b^* \propto \exp\left(\frac{Q_{\theta}(s, a^-, \hat{a}, b)}{\alpha}\right). \quad (6)$$

Since this is a global maximum solution given any sampled (s, a^-, \hat{a}) , β^* is guaranteed to be no worse than any parameterized policy. Putting β^* back into Eq. 5, we are able to simplify $V_{\theta}^{\pi^{\text{ta}}}$ (derived in Appendix B) as

$$\mathbb{E}_{\hat{a} \sim \pi_{\phi}} \alpha \left[\log \sum_{b=0}^1 \exp\left(\frac{Q_{\theta}(s, a^-, \hat{a}, b)}{\alpha}\right) - \log \pi_{\phi}(\hat{a}|s, a^-) \right]. \quad (7)$$

Then we apply the re-parameterization trick $\hat{a} = f_{\theta}(\epsilon, s, a^-)$, $\epsilon \sim \mathcal{N}(0, I)$. Approximating the gradient w.r.t. ϕ with a single sample of ϵ , we get

$$\begin{aligned} \Delta \phi &\triangleq \left(\beta_1^* \frac{\partial Q_{\theta}(s, \hat{a})}{\partial \hat{a}} - \alpha \frac{\partial \log \pi_{\phi}(\hat{a}|s, a^-)}{\partial \hat{a}} \right) \frac{\partial f_{\theta}}{\partial \phi} \\ &\quad - \alpha \frac{\partial \log \pi_{\phi}(\hat{a}|s, a^-)}{\partial \phi}. \end{aligned} \quad (8)$$

This gradient has a very similar form with SAC's (Haarnoja et al., 2018), except that here $\frac{\partial Q}{\partial \hat{a}}$ has a scaling factor of β_1^* .

Remark on multi-step actor gradient From Figure 1, one might wonder to what extent \hat{a} at the current step, if repeated as future a^- , influences the maximization of $V_{\theta}^{\pi^{\text{ta}}}$ values at future time steps. To exactly quantify this multi-step influence, starting from a replayed s_t , we need to perform a rollout of π^{ta} to estimate which future states s_{t+k} will adopt \hat{a}_t (via repeating). Let $\beta_b^*(t+k) = \beta^*(b|s_{t+k}, \hat{a}_{t+k}, a_{t+k}^-)$ be the optimal repeating policy at step $t+k$ and define $w_{t+k} = \beta_1^*(t) \prod_{k'=1}^k \beta_0^*(t+k')$ to be the probability of s_{t+k} adopting \hat{a}_t . Then the gradient term $\beta_1^* \frac{\partial Q_{\theta}}{\partial \hat{a}_t}$ in Eq. 8 should now become $\sum_{k=0}^{\infty} w_{t+k} \frac{\partial Q_{\theta}(s_{t+k}, \hat{a}_t)}{\partial \hat{a}_t}$. There are several reasons why we end up truncating this full gradient to the first step ($k=0$) as in Eq. 8:

- 1) During training we are not able to interact with the environment to get future s_{t+k} ($k \geq 1$). One solution is to use historical s_{t+k} but with importance correction.
- 2) $\frac{\partial Q_{\theta}(s_{t+k}, \hat{a}_t)}{\partial \hat{a}_t}$ has a much higher sample variance as k increases.

- 3) w_{t+k} decreases exponentially so the importance of future $\frac{\partial Q_\theta}{\partial a_t}$ quickly decays.

Our one-step truncation also results in a simple implementation of TASAC very similar to SAC.

3.4. Automatically tuned α

Similar to SAC (Haarnoja et al., 2018), given a target entropy \mathcal{H} , we learn the entropy weight α by the objective

$$\min_{\log(\alpha)} \mathbb{E}_{(s, a^-) \sim \mathcal{D}, \hat{a} \sim \pi_\phi, b \sim \beta^*} \log(\alpha) (-\log \pi_\phi(\hat{a}|s, a^-) - \log \beta_b^* - \mathcal{H}). \quad (9)$$

One difference here is that this loss adjusts $\log(\alpha)$ instead of α as in SAC, because we find directly adjusting $\log(\alpha)$ is more numerically stable. Instead of a single shared temperature, we find it beneficial to have two different temperatures for π_ϕ and β separately, which enables a finer control of the two entropy terms. Appendix C shows how our formulation slightly changes if two temperatures are used.

4. Experiments

4.1. Tasks

We perform experiments over a wide range of continuous action tasks under different scenarios, from easy to difficult:

- a) **SimpleControl**: Three classic control tasks (Brockman et al., 2016) that have very small action and/or observation spaces: *MountainCarContinuous*, *LunarLanderContinuous*, and *InvertedDoublePendulum*;
- b) **Locomotion**: Four locomotion tasks (Brockman et al., 2016) that feature complex physics and action spaces: *Hopper*, *Ant*, *Walker2d*, and *HalfCheetah*;
- c) **Terrain**: Two locomotion task that require adapting to randomly generated terrains: *BipedalWalker* and *BipedalWalkerHardcore*;
- d) **Manipulation**: Four Fetch (Plappert et al., 2018) tasks that feature sparse rewards and hard exploration manipulation (reward given only upon success): *FetchReach*, *FetchPush*, *FetchSlide*, and *FetchPickAndPlace*;
- e) **Driving**: One CARLA self-driving task (Dosovitskiy et al., 2017) that have complex high-dimensional multi-modal sensor inputs (camera, radar, IMU, collision, GPS, etc.): *Town01*. The goal is to reach a destination starting from a randomly spawned location in a large realistic town, avoiding collisions and red light violations.

Among these 14 tasks, categories (d) and (e) might benefit greatly from temporal abstraction because of hard exploration or the problem structure (e.g., driving inherently involves repeated actions). Categories (a-c) appear to have little to do with temporal abstraction, but we test if seemingly unrelated tasks can also benefit from TASAC. By comparing



Figure 3. Example tasks (out of 14) evaluated in our experiments. From left to right: *InvertedDoublePendulum*, *HalfCheetah*, *BipedalWalkerHardcore*, *FetchSlide*, and *Town01*.

TASAC against other methods across vastly different tasks, we hope to demonstrate its generality, because adaptation to this kind of task variety requires few assumptions about the task structure and inputs/outputs. Some example task screenshots are shown in Figure 3. For more task details, we refer readers to Appendix E.

4.2. Comparison methods

While there exist many off-policy hierarchical RL methods that model temporal abstraction, for example Nachum et al. (2018); Riedmiller et al. (2018); Levy et al. (2019); Li et al. (2020); Zhang et al. (2021), we did not find any of them readily scalable to our entire list of tasks (especially to high dimensional input space like CARLA). Thus we focus on comparing TASAC with several general baselines: vanilla SAC (Haarnoja et al., 2018), SAC-Nrep, SAC-Krep, and SAC-EZ, which we will explain below.

Let N be a hyperparameter representing the maximal number of action repeating steps. SAC-Nrep simply repeats every action N times. We find this simple strategy surprisingly effective in some scenarios when there exists large room for temporal abstraction. SAC-Krep, inspired by FIGAR (Sharma et al., 2017), is an extension to SAC in that the action space is augmented to a pair of (a, K) , which means that the agent will repeat action a for K steps ($1 \leq K \leq N$) without being interrupted before taking the next action pair. To implement SAC-Krep, we extended the original SAC algorithm to support a mixture of continuous and discrete actions (Appendix D). Note that SAC-Krep’s open-loop control is in contrast to TASAC’s closed-loop control. SAC-EZ incorporates the temporally extended ϵ -greedy exploration (Dabney et al., 2021) into SAC. During rollout, if the agent decides to explore, then the action is uniformly sampled and the duration for repeating that action is sampled from a truncated zeta distribution $zeta(n) \propto n^{-\mu}$, $1 \leq n \leq N$. This fixed duration model encourages persistent exploration depending on the value of the hyperparameter μ . The training step of SAC-EZ is the same with SAC.

While both SAC-Nrep and SAC-Krep introduce persistent exploration to some extent, they also have a built-in benefit of multi-step TD learning, because their immediate reward for training is actually an accumulation of environment rewards over several steps. In order to analyze the benefit of persistent exploration independent of that of multi-step

	SAC (Haarnoja et al., 2018)	SAC-Ntd	SAC-Nrep	SAC-Krep (Sharma et al., 2017)	SAC-EZ (Dabney et al., 2021)	TASAC-1td	TASAC-Ntd	TASAC
Persistent exploration	✗	✗	✓	✓	✓	✓	✓	✓
Multi-step TD	✗	✓	✓	✓	✗	✗	✓	✓
Unbiased Q operator	✓	✗	✓	✓	✓	✓	✗	✓
Closed-loop repetition	✓	✓	✗	✗	✗	✓	✓	✓
Learnable duration	✗	✗	✗	✓	✗	✓	✓	✓

Table 1. A summary of all comparison methods evaluated in our experiments. “Persistent exploration”: the ability of exploring along one action direction persistently; “Multi-step TD”: using N -step ($N > 1$) targets for TD learning; “Unbiased Q operator”: no off-policy bias in the Q operator for TD learning; “Closed-loop repetition”: the ability of terminating action repetition at any time without a duration commitment; “Learnable duration”: learning an action duration model that depends on the current state.

TD learning, we also evaluate several variants using the same value of N above. SAC-Ntd is a variant of SAC that a critic is bootstrapped by an N -step ($N > 1$) target, simply ignoring the off-policy bias. Our full method TASAC employs the unbiased multi-step Q operator $\mathcal{T}^{\pi^{\text{ta}}}$ proposed in Section 3.2 depending on the output of β , up to N steps. TASAC-1td employs a typical Bellman operator $\mathcal{B}^{\pi^{\text{ta}}}$ for one-step bootstrapping. Finally, TASAC-Ntd always bootstraps a critic with an N -step ($N > 1$) target like SAC-Ntd, regardless of β ’s outputs. Thus we have 8 methods in total for comparison in each task. See Table 1 for a summary and Appendix F for method details.

4.3. Evaluation protocol

We define *score* as the episodic return $\sum_{t=0}^T r(s_t, a_t, s_{t+1})$ of evaluating (taking $\arg \max$ of a policy) a method for a task episode, where T is a pre-defined time limit or when the episode terminates early. To facilitate score aggregation across tasks, we adopt the metric of *normalized score* (*n-score*) inspired by Mnih et al. (2015). For each task, we obtain the score (averaged over 100 episodes) of a random policy and denote it by Z_0 . We also run the trained vanilla SAC and obtain its average score Z_1 . Given any score Z , its normalized version is calculated as $\frac{Z-Z_0}{Z_1-Z_0}$. With this definition, the performance of each task category (a-e) can be computed as the aggregated normalized score across tasks within that category.

We report the mean and standard deviation of n-score curves of 3 independent random seeds. For every task, each method is trained for the same number of environment frames. Crucially, we also set up each method to train:

- for the same number of gradient steps,
- with the same mini-batch size and learning rate, and
- using roughly the same number of weight parameters,

for a fair sample efficiency comparison. A comprehensive description of experimental settings is in Appendix F.

4.4. Results

The n-score curves for all 5 task categories are shown in Figure 4. The original unnormalized score curves of all 14 tasks

are shown in Figure 8 Appendix G. Several observations can be made below.

- Multi-step TD** Even with off-policy bias, multi-step TD is better than or comparable to one-step TD (SAC-Ntd vs. SAC, TASAC-Ntd vs. TASAC-1td), except in **Locomotion**. This shows that in most cases, fast policy evaluation by multi-step trajectories outweighs its off-policy bias, and improves the overall performance. This was also observed in discrete action domains (Hessel et al., 2018).
- Naive action repetition** Naive action repetition is surprisingly effective in some scenarios while yields bad results in others (SAC-Nrep vs. SAC). When there is large room for temporal abstraction and the task does not require fine-grained control, SAC-Nrep can be much better than SAC. However, when it fails, the performance could be very bad (see *HalfCheetah* and *Ant* in **Locomotion**). Moreover, while its sample efficiency is good, usually it has a difficulty of obtaining the best scores due to its lack of flexibility in action repeating duration.
- Repeating with predicted duration lengths** With predicted duration of variable lengths, SAC-Krep is sometimes (**Locomotion**, **Manipulation**, and **Driving**) better than SAC-Nrep in terms of final performance thanks to its flexibility. However, SAC-Krep usually converges slower than SAC-Nrep because of additional multiple Q value heads to be learned for predicting repetition steps. As a result, with fewer environment frames such as in **SimpleControl** and **Terrain**, SAC-Krep hardly catches up SAC-Nrep at the end of training. While TASAC is also flexible in repeating, it does not learn additional value heads (Eq. 6). Thus it is much more efficient than SAC-Krep. More importantly, the closed-loop repetition of TASAC yields better final performance than the open-loop repetition of SAC-Krep in all task categories.
- Unbiased multi-step Q operator** Our earlier observation of multi-step TD revealed that TASAC-Ntd (with a biased Q operator) is almost always better than TASAC-1td. We can further boost the performance (TASAC vs. TASAC-Ntd) using the unbiased multi-step operator \mathcal{T}^{π} in Section 3.2. The result shows that it helps in **SimpleControl** and **Manipulation**. However, for the other

	Terrain $N=10(5)$	Manipulation $N=10(3)$	Driving $N=10(5)$
TASAC-Ntd	2.3(2.9)↓	2.7(3.2)↓	0.81(1.01)↓
TASAC	3.0(3.0)~	3.2(3.2)~	1.04(1.05)~

Table 2. Final n-scores of TASAC-Ntd and TASAC re-trained with N increased to 10. Values in parentheses are the original N values and n-scores.

three categories, TASAC-Ntd is on par with TASAC. We hypothesize that this is due to N being small (3 or 5) to accommodate SAC- $\{K,N\}$ rep which will perform poorly otherwise (due to open-loop control), and expect the off-policy-ness in TASAC-Ntd to be more as N increases. To verify this, we increased N to 10 and re-trained TASAC and TASAC-Ntd on the three categories. The final n-scores are listed in Table 2 and training curves are in Figure 9 Appendix G. We can see that as N increases, TASAC-Ntd suffers more while TASAC does not.

- 5) **Limitations** We notice that TASAC is no better than SAC on **Locomotion**. The locomotion tasks have densely shaped rewards to guide policy search. More importantly, if the agent wants to run fast, every step is critical: its joints have to precisely coordinate with each other at every moment. Thus action repetition hardly benefits this scenario, especially when the 4 tasks already have built-in frameskips (4 frames for *Hopper* and *Walker2d*; 5 frames for *Ant* and *HalfCheetah*). We believe that more complex temporal abstraction (*e.g.*, skills) is needed to improve the performance in this case. However, that TASAC is still comparable to SAC demonstrates its robustness even in unfavorable scenarios.

Combining all observations above together, the results have justified our choices of using a second-stage β policy for closed-loop action repetition, and using an unbiased Q operator conditioned on β 's output. Next, with visualization we will further analyze the importance of persistent exploration induced by action repetition.

4.5. Visualization and analysis

In this section, we use visualization techniques to qualitatively answer two questions:

- 1) How is the exploration behavior of TASAC compared to that of SAC?
- 2) What is the frequency of action repetition employed by TASAC in a well-trained control task?

4.5.1. EXPLORATION BEHAVIOR

The second-stage policy of TASAC introduces persistent exploration along previous actions, giving the agent a better chance of escaping the local neighborhood of a state when acting randomly. Thus one would imagine that TASAC's

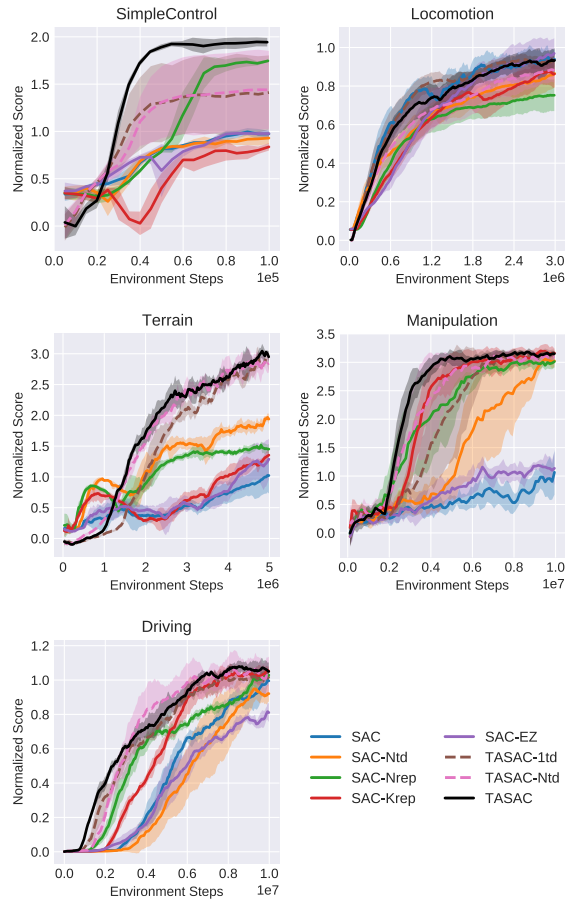


Figure 4. The n-score curves of the 5 task categories. Each curve is an aggregation of a method's performance on the tasks within a task category, where the method is run with 3 random seeds for each task. Shaded areas represent standard deviation.

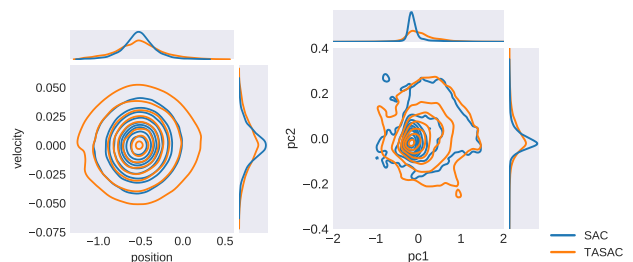


Figure 5. KDE plots of 100K (projected) state vectors visited by TASAC and SAC with their random policies. The side plots on top and right represent the estimated 1D marginal density functions. Left: *MountainCarContinuous*: x-axis is the car's position and y-axis is the car's velocity; Right: *BipedalWalker*: the axes represent the top-2 principal components of the 4D state sub-vectors representing the walker's hull statistics.

exploration yields a better state space coverage than SAC's does, assuming identical other conditions. To verify this, we visualize the state space coverages by SAC and TASAC

during their initial exploration phases of a given task.

Specifically, we select two tasks *MountainCarContinuous* and *BipedalWalker* for this purpose. For either TASAC or SAC, we play a random version of its policy on either task for 50K environment frames, to simulate the initial exploration phase where the model parameters have not yet been altered by training. During this period, we record all the 50K state vectors for analysis. For *MountainCarContinuous*, each state vector is 2D, representing the car’s “x-position” and “x-velocity” on the 1D track. For *BipedalWalker*, each state vector is 24D, where the first 4D sub-vector indicates the statistics of the walker’s hull: “angle”, “angular velocity”, “x-velocity”, and “y-velocity”. For a feasible visualization, We first extract this 4D sub-vector and form a combined dataset of 100K vectors from both TASAC and SAC. Then we apply PCA (Jolliffe, 1986) to this dataset and project each 4D vector down to 2D. After this, we are able to draw kernel density estimate (KDE) plots for both *MountainCarContinuous* and *BipedalWalker* in Figure 5. We can see that on both tasks, a random policy of TASAC is able to cover a more diverse set of states compared to that of SAC. This suggests that in general, TASAC is better at exploration thanks to its ability of persistent exploration.

4.5.2. ACTION REPETITION BY A TRAINED POLICY

In theory, to achieve optimal continuous control, the best policy should always sample an action at every step and avoid explicit action repetition at all. Thus one might assume that TASAC’s second-stage policy shifts from frequently repeating actions in the beginning of training, to not repeating actions at all towards the end of training, in order to optimize the utility. However, some action repetition examples in Figure 6 suggest that a significant repetition frequency still exists in TASAC’s top-performing evaluation episodes. Note that because we take $\arg \max$ of the policy during evaluation, this suggests that for those repeating steps, we have $\beta_0^* > \beta_1^*$ by evaluating the model.

We believe that there are at least two reasons for this surprising observation. First, with many optimization factors such as function approximation, noises in the estimated gradient, and stochasticity of the environment dynamics, it is hardly possible for a model to reach the theoretical upper bound of an utility objective. Thus for a generated action and the previous action, if their estimated Q values are very similar, then TASAC might sometimes choose to repeat. For example, in Figure 3 while the robot arm is lifting the object towards the goal in the air, it can just repeat the same lifting action for 3 steps, without altering the optimal episodic return (up to some estimation error). Similar things happen to the bipedal walker when it is jumping in the air (9 steps repeated at $t + 7$), and to the mountain car when it is rushing down the hill (11 steps repeated at $t + 26$). Second, as a

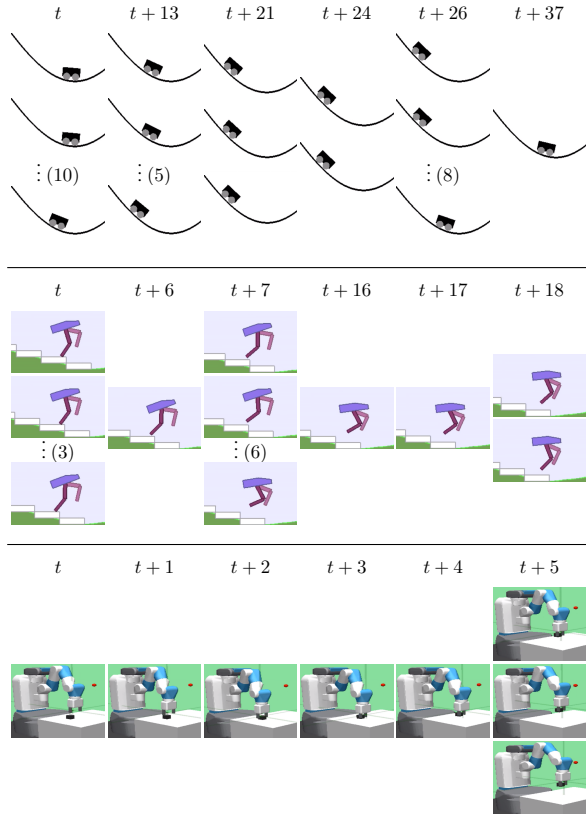


Figure 6. Example frames (zoomed in) from top-performing evaluation episodes of TASAC. Each column contains consecutive frame(s) generated by the same action, where $\vdots (n)$ denotes n similar frames omitted due to space limit. Top: *MountainCarContinuous* where the car first backs up to build gravitational potential and rushes down; Middle: *BipedalWalkerHardcore* where the walker jumps one step down; Bottom: *FetchPickAndPlace* where the robot arm approaches the object and lifts it to a goal location. function approximator, the policy network π_ϕ have a limited representational capacity, and it cannot represent the optimal policy at every state in a continuous space. For non-critical states that can be handled by repeating previous actions, TASAC might offload the decision making of π_ϕ onto β , and save π_ϕ ’s representational power for critical states. For example, the robot arm in Figure 3 invokes a fine-grained control by π_ϕ when it’s grasping the object from the table, while later does not depend on π_ϕ for lifting.

5. Conclusion

We have proposed TASAC, an off-policy RL algorithm that is a middle ground between one-level RL and hierarchical RL. TASAC incorporates closed-loop temporal abstraction into SAC by adding a second-stage policy that chooses between the previous action and a new action output by an SAC actor. The training of TASAC requires only a minor modification of that of SAC. TASAC yielded strong empirical results on a variety of continuous control tasks. The evaluation and visualization revealed the success factors of

TASAC: persistent exploration and an unbiased multi-step Q operator for TD learning. We believe that our work has provided valuable insights into modeling temporal abstraction and action hierarchies for solving complex RL tasks.

Acknowledgements

The authors would like to thank Jerry Bai and Le Zhao for helpful discussions on this project, and the Horizon AI platform team for infrastructure support.

References

- Andrychowicz, M., Wolski, F., Ray, A., Schneider, J., Fong, R., Welinder, P., McGrew, B., Tobin, J., Abbeel, P., and Zaremba, W. Hindsight experience replay. In *NeurIPS*, 2017.
- Bacon, P.-L., Harb, J., and Precup, D. The option-critic architecture. In *AAAI*, 2017.
- Brockman, G., Cheung, V., Pettersson, L., Schneider, J., Schulman, J., Tang, J., and Zaremba, W. Openai gym. *CoRR*, abs/1606.01540, 2016.
- Chen, C., Tang, H., Hao, J., Liu, W., and Meng, Z. Addressing action oscillations through learning policy inertia. In *AAAI*, 2021.
- Dabney, W., Ostrovski, G., and Barreto, A. Temporally-extended epsilon-greedy exploration. In *ICLR*, 2021.
- Dayan, P. and Hinton, G. E. Feudal reinforcement learning. In *NeurIPS*, pp. 271–278, 1993.
- Dietterich, T. G. The maxq method for hierarchical reinforcement learning. In *ICML*, pp. 118–126, 1998.
- Dosovitskiy, A., Ros, G., Codevilla, F., Lopez, A., and Koltun, V. CARLA: An open urban driving simulator. In *CoRL*, pp. 1–16, 2017.
- Duan, Y., Chen, X., Houthoofd, R., Schulman, J., and Abbeel, P. Benchmarking deep reinforcement learning for continuous control. In *ICML*, 2016.
- Fujimoto, S., van Hoof, H., and Meger, D. Addressing function approximation error in actor-critic methods. In *ICML*, pp. 1587–1596, 2018.
- Haarnoja, T., Zhou, A., Hartikainen, K., Tucker, G., Ha, S., Tan, J., Kumar, V., Zhu, H., Gupta, A., Abbeel, P., and Levine, S. Soft actor-critic algorithms and applications. *arXiv*, abs/1812.05905, 2018.
- He, K., Zhang, X., Ren, S., and Sun, J. Deep residual learning for image recognition. In *CVPR*, pp. 770–778, 2016.
- Hessel, M., Modayil, J., van Hasselt, H., Schaul, T., Ostrovski, G., Dabney, W., Horgan, D., Piot, B., Azar, M. G., and Silver, D. Rainbow: Combining improvements in deep reinforcement learning. In *AAAI*, 2018.
- Jolliffe, I. T. Principal component analysis and factor analysis. In *Principal Component Analysis*. Springer New York, 1986.
- Kingma, D. P. and Ba, J. Adam: A method for stochastic optimization. In *ICLR*, 2015.
- Lakshminarayanan, A. S., Sharma, S., and Ravindran, B. Dynamic action repetition for deep reinforcement learning. In *AAAI*, pp. 2133–2139, 2017.
- Lee, J., Lee, B.-J., and Kim, K.-E. Reinforcement learning for control with multiple frequencies. In *NeurIPS*, 2020a.
- Lee, Y., Yang, J., and Lim, J. J. Learning to coordinate manipulation skills via skill behavior diversification. In *ICLR*, 2020b.
- Levy, A., Jr., R. P., and Saenko, K. Learning multi-level hierarchies with hindsight. In *ICLR*, 2019.
- Li, A. C., Florensa, C., Clavera, I., and Abbeel, P. Sub-policy adaptation for hierarchical reinforcement learning. In *ICLR*, 2020.
- Lillicrap, T. P., Hunt, J. J., Pritzel, A., Heess, N., Erez, T., Tassa, Y., Silver, D., and Wierstra, D. Continuous control with deep reinforcement learning. In *ICLR*, 2016.
- Metelli, A. M., Mazzolini, F., Bisi, L., Sabbioni, L., and Restelli, M. Control frequency adaptation via action persistence in batch reinforcement learning. In *ICML*, 2020.
- Mnih, V., Kavukcuoglu, K., Silver, D., Rusu, A. A., Veness, J., Bellemare, M. G., Graves, A., Riedmiller, M., Fidjeland, A. K., Ostrovski, G., Petersen, S., Beattie, C., Sadik, A., Antonoglou, I., King, H., Kumaran, D., Wierstra, D., Legg, S., and Hassabis, D. Human-level control through deep reinforcement learning. *Nature*, 518(7540): 529–533, February 2015.
- Munos, R., Stepleton, T., Harutyunyan, A., and Bellemare, M. Safe and efficient off-policy reinforcement learning. In Lee, D., Sugiyama, M., Luxburg, U., Guyon, I., and Garnett, R. (eds.), *NeurIPS*, 2016.
- Nachum, O., Gu, S., Lee, H., and Levine, S. Data-efficient hierarchical reinforcement learning. In *NeurIPS*, 2018.
- Parr, R. and Russell, S. Reinforcement learning with hierarchies of machines. In *NeurIPS*, pp. 1043–1049, 1998.

- Plappert, M., Andrychowicz, M., Ray, A., McGrew, B., Baker, B., Powell, G., Schneider, J., Tobin, J., Chociej, M., Welinder, P., Kumar, V., and Zaremba, W. Multi-goal reinforcement learning: Challenging robotics environments and request for research. *arXiv*, 2018.
- Precup, D. *Temporal Abstraction in Reinforcement Learning*. PhD thesis, University of Massachusetts Amherst, 2000.
- Riedmiller, M., Hafner, R., Lampe, T., Neunert, M., Degraeve, J., van de Wiele, T., Mnih, V., Heess, N., and Springenberg, J. T. Learning by playing solving sparse reward tasks from scratch. In *ICML*, 2018.
- Schulman, J., Levine, S., Moritz, P., Jordan, M. I., and Abbeel, P. Trust region policy optimization. In *ICML*, 2015.
- Schulman, J., Wolski, F., Dhariwal, P., Radford, A., and Klimov, O. Proximal policy optimization algorithms. In *arXiv*, 2017.
- Sharma, S., Srinivas, A., and Ravindran, B. Learning to repeat: Fine grained action repetition for deep reinforcement learning. In *ICLR*, 2017.
- Sutton, R. S., Precup, D., and Singh, S. Between mdps and semi-mdps: A framework for temporal abstraction in reinforcement learning. *Artificial Intelligence*, 112(1): 181 – 211, 1999.
- Todorov, E., Erez, T., and Tassa, Y. Mujoco: A physics engine for model-based control. In *2012 IEEE/RSJ International Conference on Intelligent Robots and Systems*, pp. 5026–5033, 2012.
- Vezhnevets, A. S., Osindero, S., Schaul, T., Heess, N., Jaderberg, M., Silver, D., and Kavukcuoglu, K. Feudal networks for hierarchical reinforcement learning. In *ICML*, pp. 3540–3549, 2017.
- Wang, C., Wu, Y., Vuong, Q., and Ross, K. W. Towards simplicity in deep reinforcement learning: Streamlined off-policy learning. In *ICML*, 2020.
- Zhang, J., Yu, H., and Xu, W. Hierarchical reinforcement learning by discovering intrinsic options. In *International Conference on Learning Representations*, 2021.
- Ziebart, B. D. *Modeling purposeful adaptive behavior with the principle of maximum causal entropy*. PhD thesis, Carnegie Mellon University, 2010.

A. State value of the two-stage policy

Denoting $P(a|s, \hat{a}, a^-) \triangleq \beta_0 \delta(a - a^-) + \beta_1 \delta(a - \hat{a})$, we have

$$\begin{aligned}
 & V_\theta^{\pi^{\text{ta}}}(s|a^-) \\
 &= \int_a \pi^{\text{ta}}(a|s, a^-) Q_\theta(s, a) da \\
 &= \int_a \left[\int_{\hat{a}} \pi_\phi(\hat{a}|s, a^-) P(a|s, \hat{a}, a^-) d\hat{a} \right] Q_\theta(s, a) da \\
 &= \int_{\hat{a}} \pi_\phi(\hat{a}|s, a^-) \left[\int_a P(a|s, \hat{a}, a^-) Q_\theta(s, a) da \right] d\hat{a} \\
 &= \int_{\hat{a}} \pi_\phi(\hat{a}|s, a^-) [\beta_0 Q_\theta(s, a^-) + \beta_1 Q_\theta(s, \hat{a})] d\hat{a} \\
 &= \mathbb{E}_{\hat{a} \sim \pi_\phi, b \sim \beta} Q_\theta(s, a^-, \hat{a}, b), \\
 & \text{with } Q_\theta(s, a^-, \hat{a}, b) \triangleq (1-b)Q_\theta(s, a^-) + bQ_\theta(s, \hat{a}).
 \end{aligned}$$

B. Deriving the optimal β^* policy

In general, suppose that we have N values $X(i) \in \mathbb{R}$, $i = 0, \dots, N-1$. We want to find a discrete distribution P by the objective

$$\begin{aligned}
 & \max_P \sum_{i=0}^{N-1} P(i)(X(i) - \alpha \log P(i)), \\
 & \text{s.t. } \sum_{i=0}^{N-1} P(i) = 1,
 \end{aligned}$$

where $\alpha > 0$. Using a Lagrangian multiplier λ , we convert it to an unconstrained optimization problem:

$$\max_{P, \lambda} \sum_{i=0}^{N-1} P(i)(X(i) - \alpha \log P(i)) + \lambda \left(\sum_{i=0}^{N-1} P(i) - 1 \right).$$

Taking the derivative w.r.t. each $P(i)$ and setting it to 0, we have

$$P^*(i) = \exp\left(\frac{X(i) + \lambda - \alpha}{\alpha}\right) \propto \exp\left(\frac{X(i)}{\alpha}\right),$$

where λ is calculated to ensure $\sum_{i=0}^{N-1} P^*(i) = 1$. Furthermore, let $Z = \sum_i \exp(\frac{X(i)}{\alpha})$ be the normalizer. The resulting maximal objective is

$$\begin{aligned}
 & \sum_{i=0}^{N-1} P^*(i)(X(i) - \alpha \left(\frac{X(i)}{\alpha} - \log Z\right)) \\
 &= \sum_{i=0}^{N-1} P^*(i) \alpha \log Z \\
 &= \alpha \log Z.
 \end{aligned}$$

To derive β^* for Eq. 5 given any $(s, a^-) \sim \mathcal{D}$, $\hat{a} \sim \pi_\phi$, we set $X(0) = Q_\theta(s, a^-, \hat{a}, 0)$ and $X(1) = Q_\theta(s, a^-, \hat{a}, 1)$. Then β^* can be found as P^* above.

C. Different temperatures for β and π

In practice, we use two different temperatures α' and α'' for weighting the entropy of β and π_ϕ respectively, to have a finer control of their entropy terms. Accordingly, the objective in Eq. 5 changes to

$$\mathbb{E}_{(s, a^-) \sim \mathcal{D}, \hat{a} \sim \pi_\phi, b \sim \beta} \left[\begin{array}{l} Q_\theta(s, a^-, \hat{a}, b) \\ -\alpha' \log \beta_b - \alpha'' \log \pi_\phi(\hat{a}|s, a^-) \end{array} \right].$$

Revisiting Section 3.3, several key formulas are updated to reflect this change. Eq. 6 is updated to

$$\beta_b^* \propto \exp\left(\frac{Q_\theta(s, a^-, \hat{a}, b)}{\alpha'}\right). \quad (10)$$

Eq. 8 is updated to

$$\begin{aligned}
 \Delta \phi & \triangleq \left(\beta_1^* \frac{\partial Q_\theta(s, \hat{a})}{\partial \hat{a}} - \alpha'' \frac{\partial \log \pi_\phi(\hat{a}|s, a^-)}{\partial \hat{a}} \right) \frac{\partial f_\phi}{\partial \phi} \\
 & - \alpha'' \frac{\partial \log \pi_\phi(\hat{a}|s, a^-)}{\partial \phi}.
 \end{aligned}$$

Finally, we adjust α' and α'' separately according to their own entropy targets \mathcal{H}' and \mathcal{H}'' with two separate objectives similar to Eq. 9.

D. SAC with a mixture of discrete and continuous actions

We extend the original SAC algorithm to support a mixture of discrete and continuous actions, to implement the baseline SAC-Krep in Section 4.2. We denote the discrete and continuous actions by b ($1 \leq b \leq N$) and a , respectively. Let the joint policy be $\pi(a, b|s) = \pi(a|s)\pi(b|s, a)$, namely, the joint policy is decomposed in a way that it outputs a continuous action, followed by a discrete action conditioned on that continuous action. Let $Q_\theta(s, a, b)$ be the parameterized expected return of taking action (a, b) at state s . Then the entropy-augmented state value function is computed as

$$V_\theta^\pi(s) = \mathbb{E}_{(a, b) \sim \pi} \left[\begin{array}{l} Q_\theta(s, a, b) \\ -\alpha(\log(\pi(a|s)) + \log(\pi(b|s, a))) \end{array} \right].$$

Similar to Section 3.3, we can derive an optimal $\pi^*(b|s, a)$ given any (s, a) , and then optimize the continuous policy $\pi(a|s)$ as in Eq. 8.

For policy evaluation, in the case of SAC-Krep, b represents how many steps a will be executed without being interrupted. Thus the objective of learning Q_θ is

$$\begin{aligned}
 & \min_\theta \mathbb{E}_{(s_t, a_t, b_t, s_{t+b_t}) \sim \mathcal{D}} [Q_\theta(s_t, a_t, b_t) - \mathcal{T}^\pi Q_{\bar{\theta}}(s_t, a_t, b_t)]^2, \\
 & \text{with } \mathcal{T}^\pi Q_{\bar{\theta}}(s_t, a_t, b_t) \\
 & = \sum_{t'=t}^{t+b_t-1} \gamma^{t'-t} r(s_{t'}, a_{t'}, s_{t'+1}) + \gamma^{b_t} V_{\bar{\theta}}^\pi(s_{t+b_t}),
 \end{aligned}$$

Namely, the Q value is bootstrapped by b steps. We instantiate the Q network by having the continuous action a as an input in addition to s , and let the network output N heads, each representing $Q(s, a, b)$. An implementation of SAC with such hybrid actions is available at https://github.com/HorizonRobotics/alf/blob/pytorch/alf/algorithms/sac_algorithm.py.

E. Task details

All 14 tasks are wrapped by the OpenAI Gym (Brockman et al., 2016) interface. All of them, except *Town01*, are very standard and follow their original definitions. The environment of *Town01* is customized by us with various map options using a base map called “Town01” provided by the CARLA simulator (Dosovitskiy et al., 2017), which we will describe in detail later. We always scale the action space of every task to $[-1, 1]^A$, where A is the action dimensionality defined by the task environment. The observation space of each task is unchanged, except for *Town01*. Note that we use MuJoCo 2.0 (Todorov et al., 2012) for simulating **Locomotion** and **Manipulation**². A summary of the tasks is in Table 3.

E.1. Reward normalization

We normalize each task’s reward using a normalizer that maintains adaptive exponential moving averages of reward mean and second moment. Specifically, let ξ be a pre-defined update speed ($\xi = 8$ across all experiments), and L be the total number of times the normalizer statistics has been updated so far, then for the incoming reward r , the mean m_1 and second moment m_2 are updated as

$$\begin{aligned} \eta_L &= \frac{\xi}{L + \xi}, \\ m_1 &\leftarrow (1 - \eta_L)m_1 + \eta_L r, \\ m_2 &\leftarrow (1 - \eta_L)m_2 + \eta_L r^2, \\ L &\leftarrow L + 1, \end{aligned}$$

with $L = m_1 = m_2 = 0$ as the initialized values. Basically, the moving average rate η_L decreases according to $\frac{1}{L}$. With this averaging strategy, one can show that by step L , the weight for the reward encountered at step $l \leq L$ is roughly in proportional to $(\frac{l}{L})^{(\xi-1)}$. Intuitively, as L increases, the effective averaging window expands because the averaging weights are computed by the changing ratio $\frac{l}{L}$. Finally, given any reward r' , it is normalized as

$$\min\left(\max\left(\frac{r' - m_1}{\sqrt{m_2 - m_1^2}}, -c\right), c\right),$$

²A different version of MuJoCo may result in different observations, rewards, and incomparable environments; see <https://github.com/openai/gym/issues/1541>.

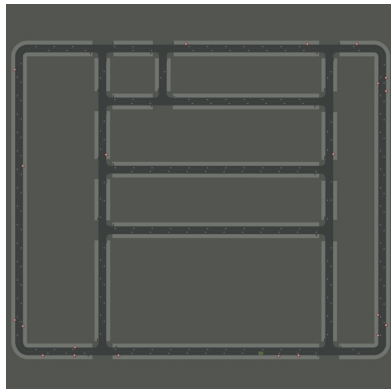


Figure 7. The layout of the map “Town01” (from <https://carla.readthedocs.io>). The actual map is filled with other objects such as buildings, trees, pedestrians, and traffic lights to make it a realistic scene of a small town.

where $c > 0$ is a constant set to either 1 or 5, according to which value produces better performance for SAC on a task. We find that the suite of **Locomotion** tasks is extremely sensitive to reward definition, and thus do not apply reward normalization to it. The normalizer statistics is updated only when rewards are sampled from the replay buffer. Note that for a task, the same reward normalization (if applied) is used by all 8 evaluated methods with no discrimination.

E.2. Town01

Our *Town01* task is based on the “Town01” map (Dosovitskiy et al., 2017) that consists of 12 T-junctions (Figure 7). The map size is roughly $400 \times 400 \text{ m}^2$. At the beginning of each episode, the vehicle is first randomly spawned at a lane location. Then a random waypoint is selected on the map and is set as the destination for the vehicle. The maximal episode length (time limit) is computed as

$$N_{\text{frames}} = \frac{L_{\text{route}}}{S_{\text{min}} \cdot \Delta t}$$

where L_{route} is the shortest route length calculated by the simulator, S_{min} is the average minimal speed expected for a meaningful driving, and Δt is the simulation step time. We set $S_{\text{min}} = 5 \text{ m/s}$ and $\Delta t = 0.1 \text{ s}$ through the experiment. An episode can terminate early if the vehicle reaches the destination, or gets stuck at collision for over a certain amount of time. We customize the map to include 20 other vehicles and 20 pedestrians that are programmed by the simulator’s built-in AI to act in the scenario. We use the default weather type and set the day length to 1000 seconds.

The action space of the vehicle is 4 dimensional: (“throttle”, “steer”, “brake”, “reverse”). We customize the observation space to include 8 different multi-modal inputs:

1. “camera”: a monocular RGB image ($128 \times 64 \times 3$)

Temporally abstract soft actor-critic for continuous control

Category	Task	Gym environment name	Observation space	Action space	Reward normalization
SimpleControl	<i>MountainCarContinuous</i>	MountainCarContinuous-v0	\mathbb{R}^2	$[-1, 1]^1$	[-5, 5]
	<i>LunarLanderContinuous</i>	LunarLanderContinuous-v2	\mathbb{R}^8	$[-1, 1]^2$	
	<i>InvertedDoublePendulum</i>	InvertedDoublePendulum-v2	\mathbb{R}^{11}	$[-1, 1]^1$	
Locomotion	<i>Hopper</i>	Hopper-v2	\mathbb{R}^{11}	$[-1, 1]^3$	×
	<i>Ant</i>	Ant-v2	\mathbb{R}^{111}	$[-1, 1]^8$	
	<i>Walker2d</i> <i>HalfCheetah</i>	Walker2d-v2 HalfCheetah-v2	\mathbb{R}^{17}	$[-1, 1]^6$	
Terrain	<i>BipedalWalker</i>	BipedalWalker-v2	\mathbb{R}^{24}	$[-1, 1]^4$	[-1, 1]
	<i>BipedalWalkerHardcore</i>	BipedalWalkerHardcore-v2			
Manipulation	<i>FetchReach</i>	FetchReach-v1	\mathbb{R}^{13}	$[-1, 1]^4$	[-1, 1]
	<i>FetchPush</i>	FetchPush-v1	\mathbb{R}^{28}		
	<i>FetchSlide</i>	FetchSlide-v1			
	<i>FetchPickAndPlace</i>	FetchPickAndPlace-v1			
Driving	<i>Town01</i>	Town01	“camera”: $\mathbb{R}^{128 \times 64 \times 3}$, “radar”: $\mathbb{R}^{200 \times 4}$, “collision”: $\mathbb{R}^{4 \times 3}$, “IMU”: \mathbb{R}^7 , “goal”: \mathbb{R}^3 , “velocity”: \mathbb{R}^3 , “navigation”: $\mathbb{R}^{8 \times 3}$ “prev action”: $[-1, 1]^4$	$[-1, 1]^4$	[-5, 5]

Table 3. The 14 tasks with their environment details. Note that reward clipping is performed after reward normalization (if applied). Except *Town01*, the input observation is a flattened vector.

- that shows the road condition in front of the vehicle;
- 2. “radar”: an array of 200 radar points, where each point is represented by a 4D vector;
- 3. “collision”: an array of 4 collisions, where each collision is represented by a 3D vector;
- 4. “IMU”: a 7D IMU measurement vector of the vehicle’s status;
- 5. “goal”: a 3D vector indicating the destination location;
- 6. “velocity”: the velocity of the vehicle relative to its own coordinate system;
- 7. “navigation”: an array of 8 future waypoints on the current navigation route, each waypoint is a 3D vector in the coordinate system of the vehicle;
- 8. “prev action”: the action taken by the vehicle at the previous time step.

Since the observation space of *Town01* is huge, we apply normalization to all input sensors for more efficient training. We normalize each input sensor vector in a similar way of reward normalization. After normalization, the vector is element-wisely clipped to $[-5, 5]$.

To train the vehicle, we define the task reward by 4 major components:

1. “distance”: a shaped reward that measures how much closer the vehicle is to the next navigation waypoint after one time step;
2. “collision”: if a collision is detected, then the vehicle gets a reward of $-\min(20, 0.5 \cdot \max(0, \bar{R}))$, where \bar{R} is the accumulated episode reward so far;
3. “red light”: if a red light violation is detected, then the

- vehicle gets a reward of $-\min(20, 0.3 \cdot \max(0, \bar{R}))$, where \bar{R} is the accumulated episode reward so far;
- 4. “goal”: the vehicle gets a reward of 100 for reaching the destination.

The overall reward at a time step is computed as the sum of the above 4 rewards. This reward definition ensures that SAC obtains reasonable performance in this task.

E.3. Network structure

The model architecture of all compared methods is identical: each trains an actor network and a critic network³. Following Fujimoto et al. (2018), the critic network utilizes two replicas to reduce positive bias in the Q function. We make sure that the actor and critic network always have the same structure (but with different weights) except for the final output layer.

Below we review the network structure designed for each task category, shared between the actor and critic network, and shared among all 8 evaluated methods. No additional network or layer is owned exclusively by any method.

- **SimpleControl**: two hidden layers, each of size 256.
- **Locomotion**: two hidden layers, each of size 256.
- **Terrain**: two hidden layers, each of size 256.
- **Manipulation**: three hidden layers, each of size 256.

³SAC-Krep actually has an extra discrete Q network that models the values of repeating $1, 2, \dots, N$ steps. It has the same structure with the critic network for the continuous action, but with multiple output heads.

Hyperparameter	SimpleControl	Terrain	Driving	Manipulation (Plappert et al., 2018)	Locomotion (Haarnoja et al., 2018)
Learning rate	10^{-4}	5×10^{-4}		10^{-3}	3×10^{-4}
Reward discount	0.99			0.98	
Number of parallel actors for rollout	1	32	4	38	
Replay buffer size per actor	10^5			2×10^4	10^6
Mini-batch size	256	4096	64	4864	
Entropy target δ (Eq. 11)	0.1			0.2	0.184
Target Q smoothing coefficient	5×10^{-3}			5×10^{-2}	
Target Q update interval	1			40	
Training interval (env frames) per actor	1	5	10	50/40	
Total environment frames for rollout	10^5	5×10^6	10^7	10^7	10^6

Table 4. The hyperparameter values of SAC on 5 task categories. The two shaded columns **Manipulation** and **Locomotion** use exactly the same hyperparameter values from the original papers, and we list them for completeness. An empty cell in the table means using the same hyperparameter value as the corresponding one of **SimpleControl**. The training interval of **Manipulation** (50/40) means updating models 40 times in a row for every 50 environment steps (per actor), which also follows the convention set by Plappert et al. (2018).

- **Driving**: We use an encoder to combine multi-modal sensor inputs. The encoder uses a mini ResNet (He et al., 2016) of 6 bottleneck blocks (without BatchNorm) to encode an RGB image into a latent embedding of size 256, where each bottleneck block has a kernel size of 3, filters of (64, 32, 64), and a stride of 2 (odd block) or 1 (even block). The encoder then flattens any other input and projects it to a latent embedding of size 256. All the latent embeddings are averaged and input to an FC layer of size 256 to yield a single encoded vector that summarizes the input sensors. Finally, the actor/critic network is created with one hidden layer of size 256, with this common encoded vector as input. We detach the gradient when inputting the encoded vector to the actor network, and only allow the critic network to learn it.

We use ReLU for all hidden activations.

F. Experiment details

F.1. Entropy target calculation

When computing an entropy target, instead of directly specifying a floating number which is usually unintuitive, we calculate it by an alternative parameter δ . If the action space is continuous, then suppose that it has K dimensions, and every dimension is bounded by $[m, M]$. We assume the entropy target to be the entropy of a continuous distribution whose probability uniformly concentrates on a slice of the support $\delta(M - m)$ with $P = \frac{1}{\delta(M - m)}$. Thus the entropy target is calculated as

$$\begin{aligned}
 & -K \int_m^M P(a) \log P(a) da \\
 & = -K \log \frac{1}{\delta(M - m)} \\
 & = K [\log \delta + \log(M - m)].
 \end{aligned} \tag{11}$$

For example, by this definition, an entropy target of -1 per dimension used by Haarnoja et al. (2018) is equivalent to setting $\delta = 0.184$ here with $M = 1$ and $m = -1$. If the action space is discrete with $K > 1$ entries, we assume the entropy target to be the entropy of a discrete distribution that has one entry of probability $1 - \delta$, with δ uniformly distributed over the other $K - 1$ entries. Thus the entropy target is calculated as

$$-\delta \log \frac{\delta}{K - 1} - (1 - \delta) \log(1 - \delta). \tag{12}$$

We find setting δ instead of the direct entropy target is always more intuitive in practice.

F.2. Hyperparameters

We use Adam (Kingma & Ba, 2015) with $\beta_1 = 0.9$, $\beta_2 = 0.999$, and $\epsilon = 10^{-7}$ to train each method. Below we first describe the hyperparameter values of the vanilla SAC baseline. These values are selected by referring to either previously published ones or our typical options for SAC runs. For **Locomotion** and **Manipulation**, we directly adopt the hyperparameter values from the original papers. Among the remaining 3 task categories (**SimpleControl**, **Terrain**, and **Driving**), several hyperparameter values vary due to task differences (Table 4). This variance also serves to test if our comparison result generalizes under different training settings.

The hyperparameter values of the other 7 evaluated methods are the same as shown in Table 4, but with extra hyperparameters if required by a method. Note that for open-loop action repetition methods like SAC-Nrep and SAC-Krep, the counting of environment frames includes frames generated by repeated actions. For the repeating hyperparameter N in Section 4.2, we set it to 3 for **SimpleControl**, **Locomotion** and **Manipulation**, and to 5 for **Terrain** and **Driving**. For SAC-EZ, we set μ of the zeta distribution to 2 following

Dabney et al. (2021), and linearly decay ϵ from 1 to 0.01 over the course of first $\frac{1}{10}$ of the training. ϵ is then kept to be 0.01 till the end of training. Finally, for the three TASAC variants (TASAC-1td, TASAC-Ntd, and TASAC), recall that the second-stage β policy requires its own entropy target (Appendix C) computed by Eq. 12. We set δ in that equation to 0.05 in all task categories except in **Locomotion** which has $\delta = 0.01$. Also in **Locomotion**, we clip the advantage $Q_\theta(s, \hat{a}) - Q_\theta(s, a^-)$ to $[0, +\infty)$ when computing β^* for the three TASAC variants.

G. More experimental results

We list the unnormalized score curves of all 14 tasks in Figure 8. The score curves are smoothed using exponential moving average to reduce noises. We notice that the scores of SAC and SAC-Nrep are still climbing considerably and approaching that of TASAC at the end of training in *Town01*. To rule out the possibility of them outperforming TASAC eventually, we train SAC, SAC-Nrep, and TASAC from scratch again to 15M environment steps (50% more steps). The updated score curves are shown in the dashed box at the bottom. We see that TASAC still performs better with more training time.

Figure 9 compares TASAC-Ntd with TASAC after N (the maximal Q bootstrapping step) is increased to 10 from 3 or 5, to show how off-policyyness introduced by TASAC-Ntd’s TD backup operator in policy evaluation degrades its training performance more as N increases. Since TASAC uses an unbiased multi-step operator, its performance is unaffected.

Temporally abstract soft actor-critic for continuous control

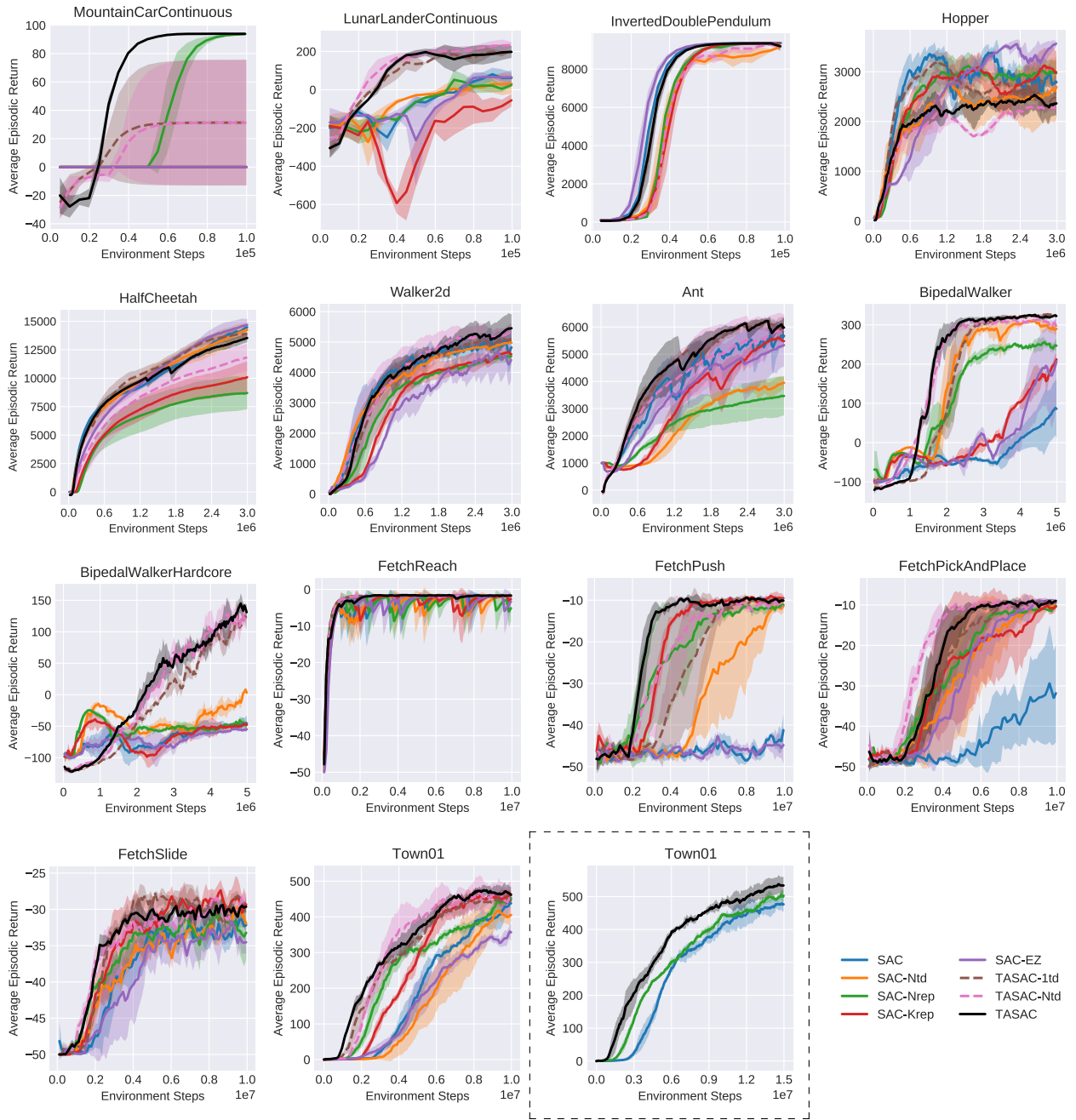


Figure 8. The unnormalized reward curves of the 14 tasks. Each curve is averaged over 3 random seeds, and shaded area represents standard deviation. The last subfigure in the dashed box runs to 15M steps to verify if SAC and SAC-Nrep have a chance of outperforming TASAC with more environment steps on *Town01*.

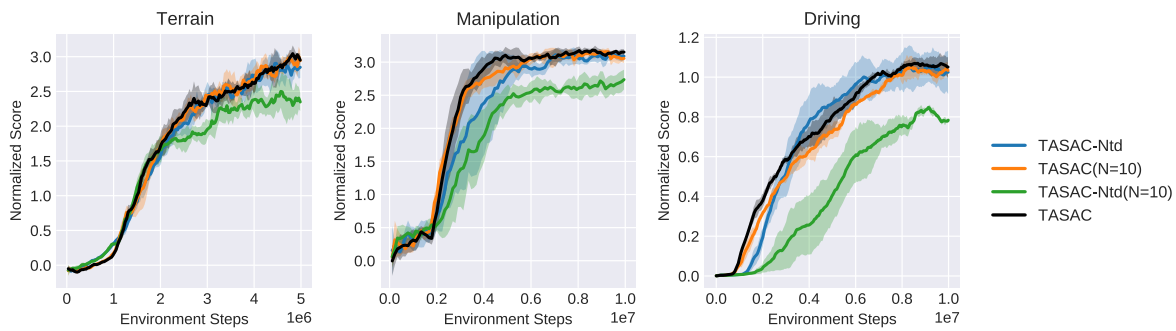


Figure 9. The n-score curves of TASAC-Ntd and TASAC on three task categories **Terrain**, **Manipulation**, and **Driving**, with $N = 10$. TASAC-Ntd becomes worse as N increases while TASAC does not. Each curve is an aggregation of a method’s performance on the tasks within a task category, where the method is run with 3 random seeds for each task. Shaded areas represent standard deviation.

H. Proof of multi-step policy evaluation convergence

We now prove that the proposed multi-step Q operator \mathcal{T}^π in Section 3.2 is unbiased, namely, Q^π is a unique fixed point of \mathcal{T}^π (policy evaluation convergence).

H.1. Operator definition

We first present a formal definition of \mathcal{T}^π . Suppose that we consider N -step ($N \geq 1$) TD learning. Each time we sample a historical trajectory $(s_0, a_0, s_1, r_{s_0, a_0, s_1}, \dots, s_N, r_{s_{N-1}, a_{N-1}, s_N})$ of $N + 1$ steps from the replay buffer to update $Q(s_0, a_0)$. For convenience, we define a sequence of auxiliary operators Γ_n^π for the V values backup recursively as

$$\begin{aligned} \Gamma_N^\pi V(\tilde{s}_N) &= \mathbb{E}_{\pi(\tilde{a}_N | \tilde{s}_N)} Q(\tilde{s}_N, \tilde{a}_N), \\ \Gamma_n^\pi V(\tilde{s}_n) &= \mathbb{E}_{\pi(\tilde{a}_n | \tilde{s}_n)} \left[\mathbb{1}_{\tilde{a}_n \neq a_n} \underbrace{Q(\tilde{s}_n, \tilde{a}_n)}_{\text{stop}} + \mathbb{1}_{\tilde{a}_n = a_n} \underbrace{\mathbb{E}_{\mathcal{P}(\tilde{s}_{n+1} | \tilde{s}_n, \tilde{a}_n)} [r_{\tilde{s}_n, \tilde{a}_n, \tilde{s}_{n+1}} + \gamma \Gamma_{n+1}^\pi V(\tilde{s}_{n+1})]}_{\text{expand}} \right], \quad 1 \leq n \leq N-1, \end{aligned} \quad (13)$$

and based on which we define

$$\mathcal{T}^\pi Q(s_0, a_0) = \mathbb{E}_{\mathcal{P}(\tilde{s}_1 | s_0, a_0)} [r_{s_0, a_0, \tilde{s}_1} + \gamma \Gamma_1^\pi V(\tilde{s}_1)]$$

as the final operator to update $Q(s_0, a_0)$. Intuitively, the above recursive transform defines a stochastic binary tree, where $\Gamma_n^\pi V(\cdot)$ are inner nodes and $Q(\cdot)$ are leaves (Figure 10). The branching of an inner node (except the last $\Gamma_N^\pi V(\tilde{s}_N)$) depends on the indicator function $\mathbb{1}_{\tilde{a}_n \neq a_n}$. From the root $\Gamma_1^\pi V(\tilde{s}_1)$ to a leaf, the maximum path length is $N + 1$ (when all $\tilde{a}_n = a_n$) and the minimum path length is 2 (when $\tilde{a}_1 \neq a_1$).

To actually estimate $\mathcal{T}^\pi Q(s_0, a_0)$ during off-policy training without access to the environment for \mathcal{P} and r , we use the technique introduced in Section 3.2 to sample a path from the root to a leaf on the binary tree, by re-using the historical trajectory as much as possible. Specifically, we first set $\tilde{s}_1 = s_1$ and $r_{s_0, a_0, \tilde{s}_1} = r_{s_0, a_0, s_1}$ as in the typical 1-step TD learning setting. Starting from $n = 1$, we sample $\tilde{a}_n \sim \pi(\cdot | s_n)$ and compare \tilde{a}_n with a_n . If they are equal, we continue to set $\tilde{s}_{n+1} = s_{n+1}$ and $r_{\tilde{s}_n, \tilde{a}_n, \tilde{s}_{n+1}} = r_{s_n, a_n, s_{n+1}}$. We repeat this process until $\tilde{a}_n \neq a_n$. In a word,

$$\mathcal{T}^\pi Q(s_0, a_0) \approx r_{s_0, a_0, s_1} + \gamma r_{s_1, a_1, s_2} + \dots + \gamma^n Q(s_n, \tilde{a}_n), \quad \tilde{a}_n \neq a_n \text{ or } n = N.$$

Usually for a continuous policy π , $\mathbb{1}_{\tilde{a}_n \neq a_n}$ is 1 with a probability of 1 because two sampled actions are always unequal. So \mathcal{T}^π will stop expanding at s_1 and it seems no more than just a normal Bellman operator for 1-step TD learning. However, if π is specially structured and has a way of generating two identical actions in a continuous space, then it has the privilege of entering deeper tree branches for multi-step TD learning. For example, TASAC is indeed able to generate \tilde{a}_n identical to the rollout action a_n if the repeating policy β outputs $b = 0$ at s_k , for all $1 \leq k \leq n$ and $n \geq 1$. In this case, $\tilde{a}_n = a_n = a_0$.

H.2. Convergence proof

We first verify that Q^π is a fixed point of \mathcal{T}^π . When $Q = Q^\pi$ in Eq. 13, we have $\Gamma_N^\pi V(\cdot) = \mathbb{E}_{\pi(\tilde{a}_N | \cdot)} Q^\pi(\cdot, \tilde{a}_N) = V^\pi(\cdot)$. Now assuming $\Gamma_{n+1}^\pi V = V^\pi$, we have

$$\begin{aligned} \Gamma_n^\pi V(\cdot) &= \mathbb{E}_{\pi(\tilde{a}_n | \cdot)} \left[\mathbb{1}_{\tilde{a}_n \neq a_n} \cdot Q^\pi(\cdot, \tilde{a}_n) + \mathbb{1}_{\tilde{a}_n = a_n} \mathbb{E}_{\mathcal{P}(\tilde{s}_{n+1} | \cdot, \tilde{a}_n)} [r_{\cdot, \tilde{a}_n, \tilde{s}_{n+1}} + \gamma V^\pi(\tilde{s}_{n+1})] \right] \\ &= \mathbb{E}_{\pi(\tilde{a}_n | \cdot)} [\mathbb{1}_{\tilde{a}_n \neq a_n} Q^\pi(\cdot, \tilde{a}_n) + \mathbb{1}_{\tilde{a}_n = a_n} Q^\pi(\cdot, \tilde{a}_n)] \\ &= \mathbb{E}_{\pi(\tilde{a}_n | \cdot)} Q^\pi(\cdot, \tilde{a}_n) \\ &= V^\pi(\cdot). \end{aligned}$$

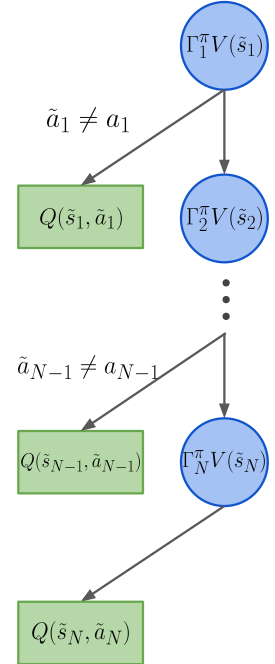


Figure 10. The stochastic binary tree defined by \mathcal{T}^π . Circles are inner nodes and rectangles are leaves. Whenever the sampled action \tilde{a}_n is not equal to the rollout action a_n , a tree path terminates.

Thus finally we have $\mathcal{T}^\pi Q^\pi(\cdot, \cdot) = \mathbb{E}_{\mathcal{P}(\tilde{s}_1|\cdot, \cdot)}[r_{\cdot, \cdot, \tilde{s}_1} + \gamma V^\pi(\tilde{s}_1)] = Q^\pi(\cdot, \cdot)$.

To prove that Q^π is the unique fixed point of \mathcal{T}^π , we verify that \mathcal{T}^π is a contraction mapping on the infinity norm space of Q . Suppose we have two different Q instantiations Q and Q' , we would like prove that after applying \mathcal{T}^π to them, $\|Q - Q'\|_\infty$ becomes strictly smaller than before. Let $\Delta = \|Q - Q'\|_\infty$ be the current infinity norm, *i.e.*, $\Delta = \max_{s,a} |Q(s, a) - Q'(s, a)|$. Then we have

$$\begin{aligned} \|\Gamma_N^\pi V - \Gamma_N^\pi V'\|_\infty &= \max_s |\Gamma_N^\pi V(s) - \Gamma_N^\pi V'(s)| \\ &= \max_s \left| \mathbb{E}_{\pi(\cdot|s)} (Q(s, \cdot) - Q'(s, \cdot)) \right| \\ &\leq \max_s \mathbb{E}_{\pi(\cdot|s)} |Q(s, \cdot) - Q'(s, \cdot)| \\ &\leq \max_s \mathbb{E}_{\pi(\cdot|s)} \Delta \\ &= \Delta, \end{aligned}$$

and for $1 \leq n \leq N - 1$ recursively

$$\begin{aligned} \|\Gamma_n^\pi V - \Gamma_n^\pi V'\|_\infty &= \max_s |\Gamma_n^\pi V(s) - \Gamma_n^\pi V'(s)| \\ &= \max_s \left| \mathbb{E}_{\pi(a|s)} \left[\mathbb{1}_{a \neq a_n} (Q(s, a) - Q'(s, a)) + \mathbb{1}_{a=a_n} \gamma \mathbb{E}_{\mathcal{P}(s'|s,a)} [\Gamma_{n+1}^\pi V(s') - \Gamma_{n+1}^\pi V'(s')] \right] \right| \\ &\leq \max_s \mathbb{E}_{\pi(a|s)} \left[\mathbb{1}_{a \neq a_n} |Q(s, a) - Q'(s, a)| + \mathbb{1}_{a=a_n} \gamma \mathbb{E}_{\mathcal{P}(s'|s,a)} |\Gamma_{n+1}^\pi V(s') - \Gamma_{n+1}^\pi V'(s')| \right] \\ &\leq \max_s \mathbb{E}_{\pi(a|s)} [\mathbb{1}_{a \neq a_n} \Delta + \mathbb{1}_{a=a_n} \gamma \Delta] \\ &\leq \max_s \mathbb{E}_{\pi(a|s)} [\mathbb{1}_{a \neq a_n} \Delta + \mathbb{1}_{a=a_n} \Delta] \\ &= \max_s \mathbb{E}_{\pi(a|s)} \Delta \\ &= \Delta. \end{aligned}$$

Finally,

$$\begin{aligned} \|\mathcal{T}^\pi Q - \mathcal{T}^\pi Q'\|_\infty &= \max_{s,a} |\mathcal{T}^\pi Q(s, a) - \mathcal{T}^\pi Q'(s, a)| \\ &= \max_{s,a} \left| \gamma \mathbb{E}_{\mathcal{P}(\cdot|s,a)} [\Gamma_1^\pi V(\cdot) - \Gamma_1^\pi V'(\cdot)] \right| \\ &\leq \gamma \max_{s,a} \mathbb{E}_{\mathcal{P}(\cdot|s,a)} |\Gamma_1^\pi V(\cdot) - \Gamma_1^\pi V'(\cdot)| \\ &\leq \gamma \max_{s,a} \mathbb{E}_{\mathcal{P}(\cdot|s,a)} \Delta \\ &= \gamma \Delta \\ &= \gamma \|Q - Q'\|_\infty. \end{aligned}$$

Since the discount factor $0 < \gamma < 1$, we have proved that \mathcal{T}^π is a contraction mapping. This shows that any Q will converge to Q^π if we repeatedly apply \mathcal{T}^π to it.